NANO LETTERS

Letter

pubs.acs.org/NanoLett

Highly Confined Tunable Mid-Infrared Plasmonics in Graphene Nanoresonators

Victor W. Brar,[†,‡] Min Seok Jang,[†] Michelle Sherrott,[†] Josue J. Lopez,[†] and Harry A. Atwater*[,†,‡]

[†]Thomas J. Watson Laboratory of Applied Physics, California Institute of Technology, Pasadena, California 91125, United States
[‡]Kavli Nanoscience Institute, California Institute of Technology, Pasadena, California 91125, United States

Supporting Information

ABSTRACT: Single-layer graphene has been shown to have intriguing prospects as a plasmonic material, as modes having plasmon wavelengths ~20 times smaller than free space ($\lambda_p \sim \lambda_0/20$) have been observed in the 2−6 THz range, and active graphene plasmonic devices operating in that regime have been explored. However there is great interest in understanding the properties of graphene plasmons across the infrared spectrum, especially at energies exceeding the graphene optical phonon energy. We use infrared microscopy to observe the modes of tunable plasmonic graphene nanoresonator arrays as small as 15 nm. We map the wavevector-dependent dispersion relations for graphene plasmons at mid-infrared energies from measurements of resonant frequency changes with nanoresonator width. By tuning resonator width and charge density, we probe graphene plasmons with $\lambda_p \leq \lambda_0/100$ and plasmon resonances as high as 310 meV (2500 cm^{-1}) for 15 nm nanoresonators. Electromagnetic calculations suggest that the confined plasmonic modes have a local density of optical states more than 10^6 larger than free space and thus could strongly increase light−matter interactions at infrared energies.

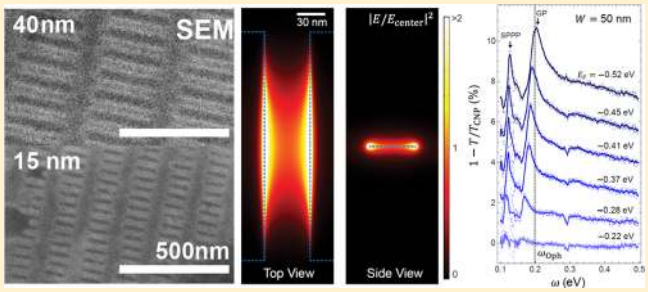

KEYWORDS: *Graphene, plasmonics, tunable resonance, graphene nanoribbon, mid-infrared, surface phonon plasmon polariton*

Surface plasmon polaritons (SPPs) are optical modes consisting of a decaying evanescent wave in a dielectric coupled to an oscillating wave of surface charge (i.e., a surface plasmon) on the surface of a conductor.[1] These modes have remarkable properties including large wavelength reductions relative to free space, and optical dispersion relations that can be engineered via metal/dielectric nanoarchitectural design. Such properties have led to interest in using SPPs for on-chip optical signal routing, visible frequency metamaterials, and as a means of increasing light-matter interactions.[2,3] While much progress has been made in achieving these goals, the use of metals as plasmonic materials has limited the capabilities of the devices. Novel metal films and nanostructures exhibit losses due to low carrier mobilities, surface roughness, grain microstructure and impurities,[4] and the large electronic density of states in metals restricts the possibility of dynamically tuning the plasmon energy via externally applied electrostatic fields. These limitations have led to a search for alternative plasmonic materials, including transparent conducting oxides, transition metal nitrides, superconductors, and graphene.[5,6]

Single layer graphene has interesting prospects as a plasmonic material. It has been shown theoretically and experimentally that SPPs excited in finite thickness metal films embedded in dielectrics or metal-clad dielectric slots display smaller mode volumes as the middle layer becomes thinner.[7−13] A single atomic layer of material, such as graphene, represents the ultimate limit of this trend, and theoretical predictions have shown that the mode volumes of SPPs in graphene can be 10^6 times smaller than those in free space.[14−16] Furthermore, the dielectric properties of graphene can be dynamically tuned by chemical or electrostatic changes to the charge density of the graphene sheet.[14,17] This allows for the creation of SPP based devices that can be effectively turned on and off or tuned to be active at different frequencies. Such devices have recently been demonstrated in the THz regime on graphene samples patterned at micrometer length scales, demonstrating plasmonic wavelengths ~20 times smaller than free space ($\lambda_p \sim \lambda_0/20$) and 0.3 decades of tunability in the 2−6 THz range.[18−20] In the infrared regime some progress has also been made in imagining plasmons using 10 μm wavelength scattering NSOM techniques, revealing graphene plasmons 50−60 times smaller than the free space wavelength,[21,22] and very recently graphene nanostructures with ion gel topgates on indium tin oxide substrates were investigated in the mid-infrared regime.[23] However, there is still great interest in understanding the properties of graphene plasmons across the infrared spectrum. Some theoretical work has predicted that graphene plasmons in the infrared should display long lifetimes and high mode confinement,[15] while another work has predicted that graphene is too lossy to exhibit strong plasmonic

Received: February 15, 2013
Revised: April 11, 2013
Published: April 26, 2013

 © 2013 American Chemical Society dx.doi.org/10.1021/nl400601c | *Nano Lett.* 2013, 13, 2541−2547

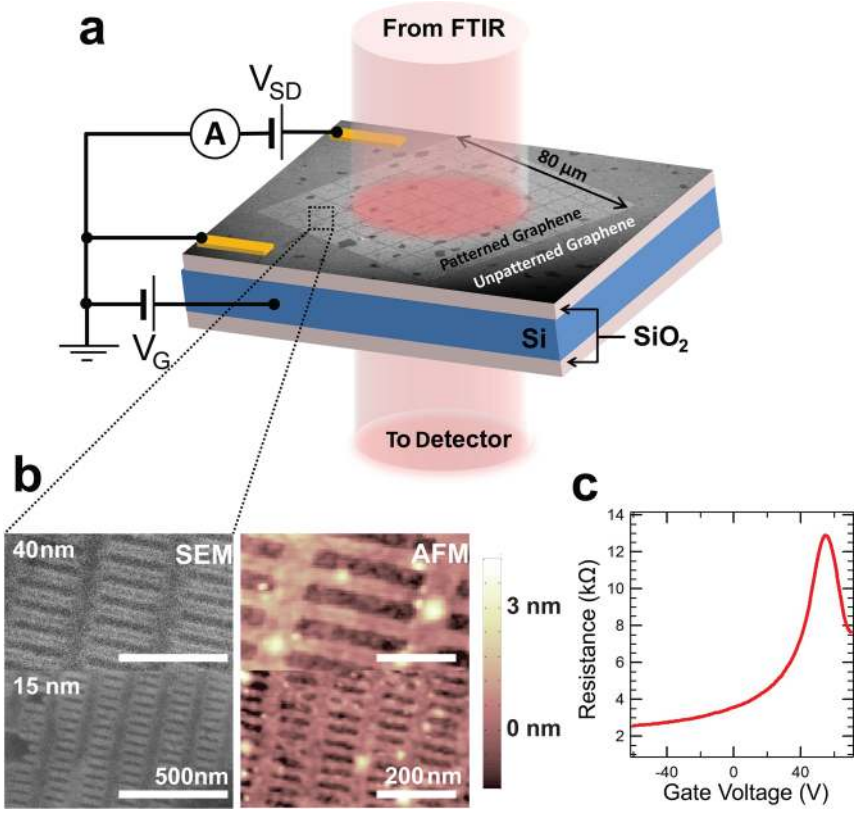

Figure 1. Schematic of experimental device. (a) SEM image of a 80 × 80 um^2 graphene nanoresonator array etched in a continuous sheet of CVD graphene. The graphene sheet was grounded through Au(100 nm)/Cr(3 nm) electrodes that also served as source−drain contacts, allowing for in situ measurements of the graphene sheet conductivity. A gate bias was applied through the 285 nm SiO_2 layer between the graphene sheet and the doped Si wafer (500 um thick). FTIR transmission measurements were taken over a 50 μm diameter spot. (b) SEM and AFM images of 40 and 15 nm graphene nanoresonator arrays. A nanoresonator width uncertainty of ±2 nm was inferred from the AFM measurements. (c) A resistance vs gate voltage curve of the graphene sheet showing a peak in the resistance at the charge neutral point (CNP), when the Fermi level (E_F) is aligned with the Dirac point.

properties in the mid-infrared, especially at energies above the 200 meV optical phonon energy of graphene.[5]

In this work we use infrared microscopy to measure the plasmon resonances of graphene nanoresonator arrays patterned down to 15 nm length scales on a back-gated graphene device. By probing how the resonant frequency changes with nanoresonator width, we are able to map the wavevector-dependent dispersion relations of graphene plasmons in the mid-infrared regime. We further show how the graphene plasmon dispersion relation changes as the charge density is continuously varied, and we find that the mode volume, intensity, and frequency of plasmon modes depend strongly on the graphene charge density. By tuning these parameters (nanoresonator width and charge density) we create and probe plasmons in graphene with $\lambda_p \leq \lambda_0/100$, and resonant energies as high as 310 meV (2500 cm^{-1}) for 15 nm nanoresonators. By comparing our results to finite element electromagnetic simulations, we find that these confined plasmonic modes have mode densities more than 10^6 larger than free space and thus could serve and an effective means for increased light−matter interactions. Finally, we observe additional and unexpected resonances in the graphene nanoresonator spectrum around 110 meV (900 cm^{-1}). These features can be effectively modeled as surface plasmon phonon polaritons (SPPPs),[24,25] new fundamental excitations that arise due to strong coupling between the graphene plasmons and the optical phonons of the SiO_2 substrate.

A schematic of our experimental setup is shown in Figure 1a. Our measurements were performed on graphene grown on 25 μm thick copper foil using established chemical vapor deposition growth techniques.[26,27] After being transferred to SiO_2/Si wafers, nanoresonator arrays were patterned in the graphene using 100 keV electron beam lithography in PMMA followed by an oxygen plasma etch. Using this process we were able to fabricate graphene nanoresonators over 80 × 80 μm^2 areas with widths varying from 80 nm to 15 nm. The aspect ratio of the nanoresonators was 5−8:1 and the period was 2−3× (width). Figure 1b shows scanning electron microscope (SEM) and atomic force microscope (AFM) images of the graphene nanoresonators after fabrication. A typical gate-dependent resistance curve for one of our devices is shown in Figure 1c. The peak in the resistance corresponds to the charge neutral point (CNP) of the graphene, when the Fermi level is aligned with the Dirac point and the carrier density is minimized.[28] After the CNP for each device was measured, a capacitor model[28] was used to determine the Fermi level position for each applied gate voltage (see Supporting Information).

Transmission measurements were done in a Fourier transform infrared (FTIR) microscope using a 50 μm diameter spot size and with light polarized perpendicular to the graphene nanoresonators. In order to probe carrier-dependent optical properties of the graphene nanoresonators all spectra were normalized to spectra taken at the charge neutral point. Figure

dx.doi.org/10.1021/nl400601c | Nano Lett. 2013, 13, 2541−2547

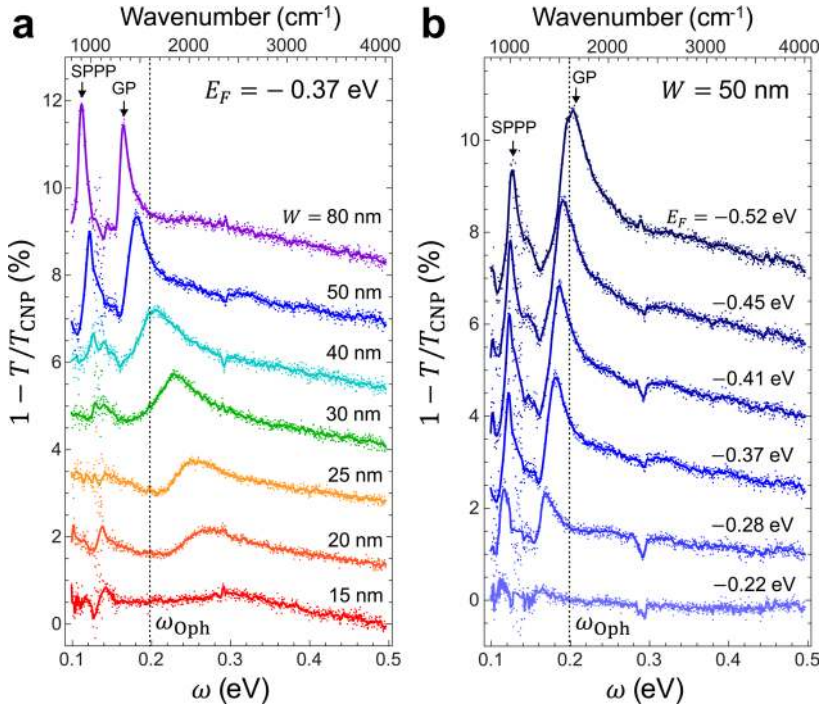

Figure 2. Gate-induced modulation of transmission through graphene nanoresonator arrays normalized to transmission spectra obtained at the CNP. (a) Width dependence of optical transmission through graphene nanoresonator arrays with E_F = −0.37 eV. The width of the nanoresonators is varied from 15 to 80 nm. (b) Fermi level dependence of optical transmission through 50 nm wide graphene nanoresonators, with E_F varying from −0.22 to −0.52 eV. The dotted vertical line in both a and b indicates the zone-center energy of the in-plane optical phonons of graphene.

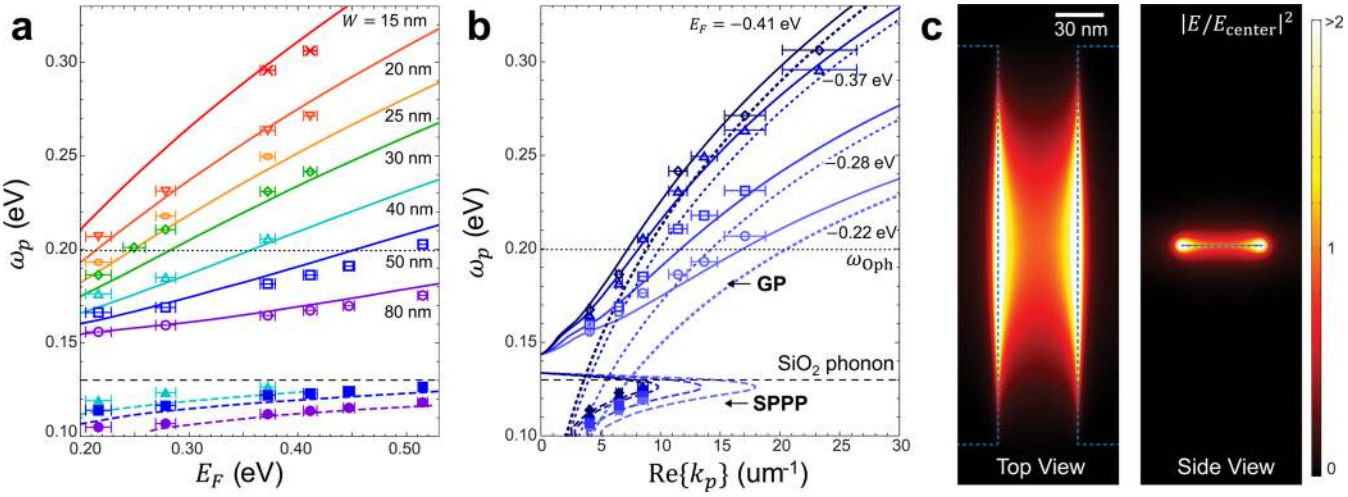

Figure 3. Dispersion of GP and SPPP plasmonic resonances in graphene nanoresonator arrays. (a) Fermi level dependence of the measured energy of "GP" (open colored symbols) and "SPPP" (filled colored symbols) features observed in nanoresonators with varying widths. Solid and dashed colored lines indicate the two solutions to eq 1 using the same experimental widths and continuously varying E_F. (b) Theoretical dispersion of bare graphene/SiO_2 plasmons (solid) and SPPPs (dashed), for different E_F values. Open and filled symbols plot the measured energy of "GP" and "SPPP" features (respectively) from graphene nanoresonators at equivalent E_F values. Wavevector values for experimental points are obtained from AFM measurements of the nanoresonator widths followed by a finite elements simulation to calculated the wavelength of the first order supported plasmon modes. The dotted blue lines indicate the theoretical plasmon dispersion of graphene on a generic, nondispersive dielectric with ε_∞ = 2.1, which is the high frequency permittivity of SiO_2. Dashed and dotted black lines in a and b indicate the energy of the TO optical phonon of SiO_2 and the zone-center energy of the in-plane optical phonons of graphene, respectively. (c) Mode profile of the GP mode of a 50 nm graphene nanoresonator with E_F = −0.37 eV, obtained from a finite element electromagnetic simulation.

2a shows normalized spectra taken from nanoresonator arrays with widths varying from 80 to 15 nm while the Fermi level is held at −0.37 eV, corresponding to a carrier density of 8.8 × 10^{12} holes per cm^2. These spectra contain two different types of features. The first is a surface plasmon phonon polaritons, labeled SPPP, which is a sharp resonance that appears near 0.12 eV for the 80 nm and 50 nm nanoresonators but is not visible for nanoresonators with widths <40 nm. The second feature is the graphene plasmon, labeled GP, which is a broader peak that appears for all nanoresonator widths. As the width of the nanoresonators is decreased, the energy and width of the GP peak increase, while the intensity of this feature decreases. For

dx.doi.org/10.1021/nl400601c | Nano Lett. 2013, 13, 2541−2547

example, for 80 nm nanoresonators this feature appears as a narrow peak at 0.16 eV, while for 15 nm nanoresonators it appears as a very weak and broad peak at 0.29 eV.

To better understand the origin of these two features, we monitored how they changed as we varied the carrier density of the graphene sheet. Figure 2b shows a series of spectra taken in this manner from 50 nm nanoresonator arrays. For low carrier densities, when E_F is only 0.22 eV below the Dirac point, both SPPP and GP peaks appear very weakly in the nanoresonator spectrum, at 0.114 and 0.166 eV, respectively. As more carriers are added to the graphene sheet, both SPPP and GP peaks gain intensity and shift to higher frequencies, with the SPPP and GP reaching 0.126 and 0.203 eV, respectively, when E_F is increased to 0.52 eV below the Dirac point. In Figure 3a we plot the SPPP and GP peak energies for all nanoresonator widths as a function of E_F. Here we observe that the energy of the GP feature shows a stronger dependence on carrier density for smaller nanoresonator widths.

These two experimentally observed resonances can be understood using a simple Fabry–Perot model of plasmons bound in graphene nanoresonators patterned on SiO_2. When incident light is coupled to a graphene plasmon mode of the wavevector k_p, the plasmon undergoes multiple reflections between the two edges of the nanoresonator. Constructive interference occurs when the reflected plasmons are in phase, which occurs when $2\,\mathrm{Re}\{k_p\}W + 2\phi = 2m\pi$, where W is the width of the nanoresonator and ϕ is the phase shift of the plasmons upon reflection. We estimated ϕ by performing electromagnetic simulations using a finite element method and for the first-order resonance ($m = 1$), ϕ is calculated to be 0.30π to 0.35π depending on the width to period ratio. This implies that the plasmon wavelength $\lambda_p = 2\pi/\mathrm{Re}\{k_p\}$ is almost three times that of the nanoresonator width. Interestingly, we note that ϕ is scale-invariant, as long as the system is in the electrostatic limit ($k_p \gg \omega_p/c$).[29] Recognizing that the wavevector k_p can be approximated to $i\bar{\varepsilon}\omega_p/[2\pi\sigma(\omega_p)]$ in the electrostatic limit,[15] the condition for the first-order plasmon resonance is reduced to

$$\frac{\omega_p W}{2\pi}\mathrm{Im}\left\{-\frac{\bar{\varepsilon}(\omega_p)}{\sigma(\omega_p)}\right\} = \pi - \phi \tag{1}$$

Here, $\bar{\varepsilon}(\omega) = (1 + \varepsilon_{SiO_2}(\omega))/2$ is the average dielectric function of the air–SiO_2 interface. In our calculations, we used an analytic expression for the graphene conductivity $\sigma(\omega)$ evaluated within the local random phase approximation,[30] and the complex dielectric function of SiO_2, $\varepsilon_{SiO_2}(\omega)$, was taken from Palik.[31]

Upon solving eq 1 we find that for some graphene nanoresonator widths multiple first-order plasmon modes can be supported. This effect is due to the dispersive permittivity of SiO_2, which varies greatly near its transverse optical phonon at 0.13 eV. This results in two separate bands in the graphene/SiO_2 plasmon dispersion relation, both of which can create plasmon resonances in the patterned graphene. In Figure 3a we plot as solid and dashed lines the resonant energies of these two modes for different nanoresonator widths and E_F values, showing that one of the modes (solid line) has a width and carrier density dependence that correlates well with the GP feature, while the other mode (dashed line) behaves like the SPPP feature. We note that, in principle, there can be a third solution to eq 1 that would occur almost right at the SiO_2 phonon energy, however, this mode is heavily damped by the substrate lattice oscillations.

From these calculations, we can now explain the physical origins of the GP and SPPP features observed in our data. The graphene plasmon mode corresponds to a confined plasmon excitation of a monolayer graphene sheet in a nearly constant dielectric environment. As described in previous work,[14,15,18,22] when the frequency (ω_p) of such modes are sufficiently lower than the interband transition energy ($2|E_F|$), ω_p should depend on both carrier density and nanoresonator width through the relationship $\omega_p \propto |E_F|^{1/2}W^{-1/2}$. This behavior is demonstrated by the graphene plasmon mode in Figure 3a, although it deviates slightly at lower energies. At energies sufficiently far from the SiO_2 phonon energy, the dispersion relation of this mode (Figure 3b, solid lines) is seen to asymptotically approach the dispersion of graphene plasmons on a generic and nondispersive dielectric substrate.

The SPPP modes can be understood by considering that lattice oscillations in the SiO_2 leads to a sharp increase in the SiO_2 dielectric constant below its phonon energy. Because the graphene plasmon wavelength depends on the surrounding dielectric environment (see eq 1), the high dielectric constant of the SiO_2 within the small energy range below the phonon can compress graphene plasmons and allow for the graphene nanoresonators to support additional low energy plasmon oscillations. Thus this mode represents a composite excitation that consists of a SPP on the graphene coupled to a phonon excitation in the SiO_2, hence the term surface plasmon phonon polariton (SPPP). Signatures of such plasmon–phonon coupling have previously been observed in NSOM measurements of graphene on SiO_2 surfaces.[32] In Figure 3b we plot the dispersion relation for this SPPP (dashed lines) for different Fermi energies, revealing that the SPPP mode displays less dispersion than the graphene plasmon mode. Another notable feature of the SPPP that can be observed in the dispersion curve is that modes with high-k vectors are not supported. This can be understood by considering that, while the SiO_2 phonon changes the dielectric function of the substrate, it also introduces loss. Thus as the energy of the SPPP moves closer to the SiO_2 phonon energy, the system becomes too lossy due to substrate absorption, and these modes can no longer propagate.

The most remarkable feature of both the graphene plasmon and SPPP resonances is how small the supported plasmon wavelengths are compared to the free space wavelength λ_0. For example, when $E_F = -0.22$ eV we observe for the graphene plasmon feature that $\lambda_0/\lambda_p = 49$ in the 50 nm wide nanoresonators, and λ_0/λ_p becomes as large as 106 in the 20 nm nanoresonators, as summarized in Figure 4a. This factor is seen to decrease as the carrier density of the graphene sheet is increased and the graphene nanoresonators support higher energy resonances, such that for $E_F = -0.41$ eV, we measure λ_0/λ_p of 43 and 81 for 50 and 20 nm nanoresonators, respectively. These results are largely consistent with the theoretical predictions of infrared graphene plasmons.[15] The SPPP mode similarly displays large wavelength reductions, reaching $\lambda_0/\lambda_p = 71$ for 50 nm nanoresonators when $E_F = -0.22$ eV and $\lambda_0/\lambda_p = 66$ for $E_F = -0.41$ eV.

These small plasmon wavelengths have interesting implications for light–matter interactions on graphene nanoresonators, by considering for example the Purcell factor, which describes spontaneous emission modified by coupling to an optical cavity.[33] The spontaneous emission enhancement is

dx.doi.org/10.1021/nl400601c | Nano Lett. 2013, 13, 2541–2547

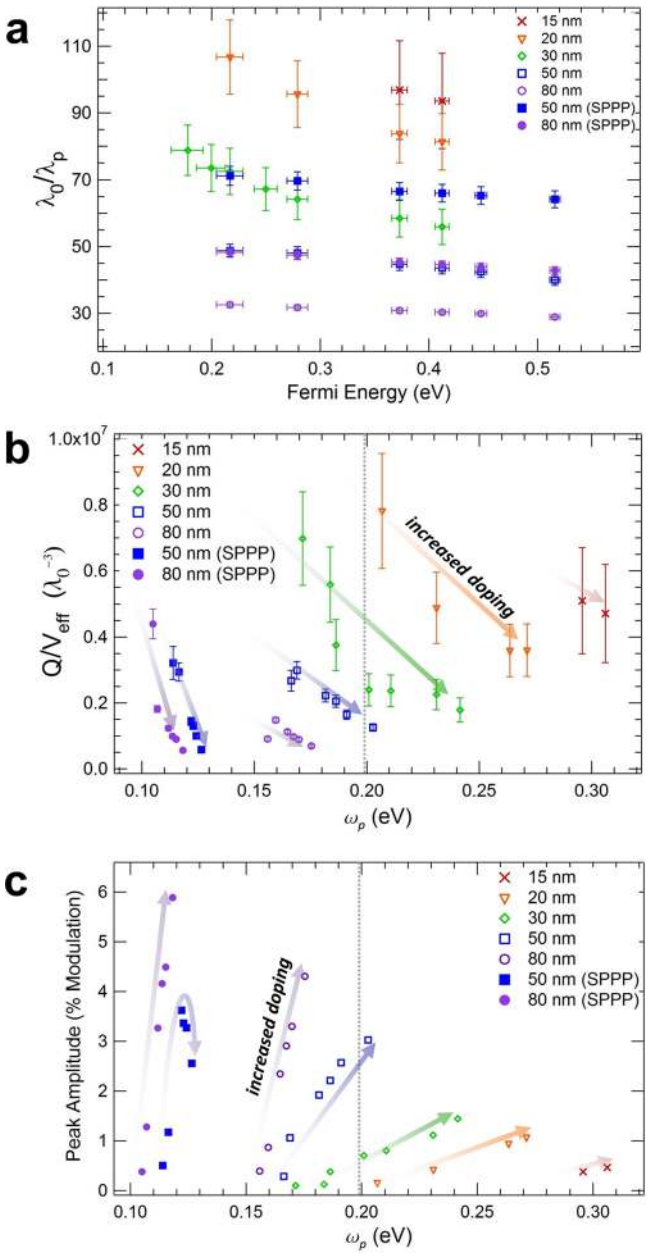

Figure 4. Properties of plasmonic modes in graphene nanoresonators. (a) Wave localization (λ_0/λ_p) of graphene plasmons and SPPP's bound in nanoresonators of different widths, plotted as a function of E_F. The plasmon wavelength is obtained by considering the constructive interference of plasmons scattering from the ribbon edges, with the ribbon width obtained from AFM measurements. (b) Q/V_{eff} for GP and SPPP modes observed in graphene nanoresonators of different characteristic widths and E_F values. Q is derived from the measured spectra as the ratio of the resonance frequency to the peak width ($\omega_p/\Delta\omega$), and V_{eff} is obtained from the AFM measured geometric dimensions of the nanoresonators by electromagnetic simulations using a finite element method. (c) Amplitude of transmission modulation through graphene nanoresonators of varying width and E_F.

proportional to Q/V_{eff}, where Q is the quality factor and V_{eff} is the effective mode volume normalized by the free space mode volume λ_0^3. The quality factor of our devices is estimated from measured spectra as the ratio of the resonance frequency to the peak width ($Q \approx \omega_p/\Delta\omega$), giving a value that ranges from 2.5 to 15, which is relatively low for an optical cavity. However the large wavelength confinement observed here ($\lambda_0/\lambda_p \sim 100$) is consistent with a mode volume V_{eff} for a single nanoresonator that is extremely small. Thus the overall enhancement factor Q/V_{eff} is quite high. In order to explore this possibility, we calculate V_{eff} for the graphene plasmon and SPPP modes measured in this work by employing three-dimensional finite element electromagnetic simulations. We first note that the electric field is tightly confined near the nanoresonator as shown in Figure 3c. Because our system is in the electrostatic limit ($k_p \gg \omega_p/c$), the out-of-plane decay length, $(k_p^2 - \varepsilon\omega_p^2/c^2)^{-1/2}$, is nearly equal to k_p^{-1} regardless of the resonance frequency ω_p or the permittivity ε. Thus considering $k_p^{-1} \sim W$, $W^2 \times$ length can be regarded as a good estimate of the mode volume. The rigorous definition of the effective mode volume, which we calculate here, is given by $V_{eff} = \int u\, dV/u_0$, where the numerator is the total stored energy and u_0 is the electromagnetic-energy density at the emitter position.[34] For our calculation, we assume that the emitter sits at the center of the resonator, right on top of graphene sheet. We display the result of these calculations in Figure 4b, which shows that for both the graphene plasmon and SPPP modes, the value Q/V_{eff} is in the range 10^6–$10^7\lambda_0^{-3}$. This represents a 2 orders of magnitude increase over what has so far been achieved using plasmon modes confined on metal nanowires.[35,36] It is interesting to point out that Q/V_{eff} continues to get larger as W is decreased for the same E_F. This occurs despite the fact that ω_p moves above the frequency threshold ω_{Oph} where optical phonon scattering of plasmons can occur and also regardless of the fact that the nanoresonator edge roughness dampens the plasmons more efficiently as the resonators become smaller. Both of those effects lead to a lower Q value, but they are offset by the increased mode confinement (i.e., smaller V_{eff}). We also observe that Q/V_{eff} decreases as the charge density of the graphene sheet increases. This is due to the increase in energy of the supported plasmonic modes as we raise E_F, which leads to a larger V_{eff}. It should be also noted that our nanoresonators support additional higher order modes that have nodes in the longitudinal direction yet are first-order in transverse direction. Because these higher order modes have resonance frequencies close to ω_p of the fundamental mode and their spectral widths are finite, these modes can further increase the local density of optical states at $\omega = \omega_p$. Consequently, the actual spontaneous emission enhancement could be higher than the value estimated by merely considering the fundamental mode.

Finally, in Figure 4c we analyze the modulated transmission intensity due to the plasmonic modes supported on the nanoresonators. In contrast to the Purcell factor of our resonators, the intensity of the plasmon oscillations generally increases as $|E_F|$ becomes higher. This can be attributed to two effects. First, as E_F is increased, more charge carriers interact with the incident electromagnetic wave, and thus the overall strength of the plasmon resonance is increased.[18] Second, the wavelength mismatch (λ_0/λ_p) is decreased for higher carrier densities, which leads to a better coupling from free space light to surface plasmons. In contrast to the other modes, the SPPP mode of the W = 50 nm resonators deviates from this general trend. For high carrier density, its resonant frequency approaches too close to the SiO_2 phonon energy, and lifetime reduction due to SiO_2 phonon damping dominates all the other effects. Finally, we note that the resonance intensity becomes smaller for narrower nanoresonators. This can be explained by both increase in edge roughness-to-width ratio and the plasmon-optical phonon scattering at $\omega_p > \omega_{Oph}$.

dx.doi.org/10.1021/nl400601c | Nano Lett. 2013, 13, 2541–2547

We have experimentally demonstrated that graphene nanoresonators in the 15−80 nm size range can support multiple plasmonic resonances that interact with mid-infrared light. We find that, as nanoresonators are made smaller, the plasmon frequency becomes more sensitive to the sheet charge density, and thus for the small features studied here the resonances could be moved over a large frequency range using only an electrostatic back-gate. The large wavelength mismatches we observe between the plasmonic modes and free space photons imply that an emitter near the surface of the nanoresonators should experience a large Purcell enhancement in the 10^6−10^7 range. Increasing the graphene charge density can decrease this strong interaction. However a higher charge density allows free space light to more efficiently couple to the plasmonic modes. This trade-off has important implications for achieving large increases in the spontaneous emission rate in the vicinity of graphene.

Methods. *Device Fabrication.* Following CVD graphene growth, the Cu foil was etched in iron chloride and ammonium persulfate solutions, and the graphene was transferred to double-side polished oxidized Si wafers with 285 nm SiO_2 on 10 Ohm-cm Si using either a polydimethylsiloxane (PDMS) stamp or a poly(methyl methacrylate) (PMMA) transfer technique. Nanoresonator arrays were patterned in the graphene using 100 keV electron beam lithography on 90−300 nm thick 950 PMMA (MicroChem). The exposed PMMA was developed in 3:1 isopropanol:methyl isobutyl ketone (MIBK) for 45 s, and the pattern was etched into the graphene using oxygen plasma at 20 mTorr and 80 W for 10 s. In order to tune and monitor the carrier density of our device in situ, source and drain contacts (3 nm Cr, 100 nm Au) were deposited on the bare graphene areas adjacent to the nanoresonator arrays, and the sample was connected in a field effect transistor (FET) configuration, with the Si layer acting as the backgate electrode.

Electromagnetic Simulations. We rigorously solve Maxwell's equation by using the finite element method. We modeled graphene as a thin film of the thickness δ and impose the relative permittivity $\varepsilon_G = 1 + 4\pi i\sigma/\omega\delta$. $\sigma(\omega)$ is the complex optical conductivity of graphene evaluated within the local random phase approximation.[30] δ is chosen to be 0.1 nm which shows good convergence with respect to the $\delta \to 0$ limit. The complex dielectric function of SiO_2, $\varepsilon_{SiO_2}(\omega)$, was taken from Palik.[31]

Electric Energy Density. The well-known relation for energy density $u = \varepsilon|E|^2/16\pi$, where ε is the dielectric constant of the material and $|E|^2$ is the electric field intensity, is valid only for nondispersive materials, and thus not applicable to graphene and SiO_2. In this work, we adopt the energy density defined in ref 34, $u = (\mathrm{Re}\{\varepsilon\} + 2\omega\mathrm{Im}(\varepsilon)/\Gamma)|E|^2/16\pi)$, which is appropriate for Drude materials with permittivity $\varepsilon = \varepsilon_\infty - \omega_0^2/[(\omega^2 - \omega_r^2) + i\Gamma\omega]$. For SiO_2, the parameters are fitted to the data taken from Palik,[31] resulting in $\varepsilon_\infty = 2.11$, $\omega_0 = 0.111$ eV, $\omega_r = 0.132$ eV, and $\Gamma = 0.00882$ eV. The dielectric function of graphene is also well-described by the Drude model when ω is much lower than the interband threshold $2E_F$.[30]

■ ASSOCIATED CONTENT

Supporting Information

Approximating the Fermi level position, plasmon lifetime, and supporting figures. This material is available free of charge via the Internet at http://pubs.acs.org.

■ AUTHOR INFORMATION

Corresponding Author

*E-mail: haa@caltech.edu.

Author Contributions

V.W.B. and M.S.J. contributed equally.

Notes

The authors declare no competing financial interest.

■ ACKNOWLEDGMENTS

While preparing this manuscript, we became aware of two recent works studying mid-infrared plasmon resonances on graphene.[23,37] The authors gratefully acknowledge support from the Air Force Office of Scientific Research Quantum Metaphotonic MURI program under grant FA9550-12-1-0488 and use of facilities of the DOE "Light-Material Interactions in Energy Conversion" Energy Frontier Research Center (DE-SC0001293). V.W.B. gratefully acknowledges a postdoctoral fellowship from the Kavli Nanoscience Institute. The authors are thankful for helpful discussions with J. Fakonas, S. Burgos, S. Kim, L. Ju, R. Weitekamp, E. Kosten, M. Sheldon, and D. Callahan.

■ ABBREVIATIONS

SPP, surface plasmon polariton; SPPP, surface plasmon phonon polariton; FTIR, Fourier transform infrared spectroscopy; CVD, chemical vapor deposition; CNP, charge neutral point

■ REFERENCES

(1) Raether, H. *Surface plasmons on smooth and rough surfaces and on gratings*; Springer-Verlag: Berlin, 1988; p *x*.
(2) Polman, A. *Science* **2008**, *322* (5903), 868−869.
(3) Chang, D. E.; Sorensen, A. S.; Hemmer, P. R.; Lukin, M. D. *Phys. Rev. Lett.* **2006**, *97* (5), 053002.
(4) Nagpal, P.; Lindquist, N. C.; Oh, S.-H.; Norris, D. J. *Science* **2009**, *325* (5940), 594−597.
(5) Tassin, P.; Koschny, T.; Kafesaki, M.; Soukoulis, C. M. *Nat. Photonics* **2012**, *6* (4), 259−264.
(6) Boltasseva, A.; Atwater, H. A. *Science* **2011**, *331* (6015), 290−291.
(7) Berini, P. *Opt. Lett.* **1999**, *24* (15), 1011−1013.
(8) Dionne, J. A.; Sweatlock, L. A.; Atwater, H. A.; Polman, A. *Phys. Rev. B* **2005**, *72* (7), 075405.
(9) Miyazaki, H. T.; Kurokawa, Y. *Phys. Rev. Lett.* **2006**, *96* (9), 097401.
(10) Kliewer, K. L.; Fuchs, R. *Phys. Rev.* **1967**, *153* (2), 498−512.
(11) Economou, E. N. *Phys. Rev.* **1969**, *182* (2), 539.
(12) Sarid, D. *Phys. Rev. Lett.* **1981**, *47* (26), 1927−1930.
(13) Burke, J. J.; Stegeman, G. I.; Tamir, T. *Phys. Rev. B* **1986**, *33* (8), 5186−5201.
(14) Hwang, E. H.; Das Sarma, S. *Phys. Rev. B* **2007**, *75* (20), 205418.
(15) Jablan, M.; Buljan, H.; Soljacic, M. *Phys. Rev. B* **2009**, *80* (24), 245435.
(16) Koppens, F. H. L.; Chang, D. E.; de Abajo, F. J. G. *Nano Lett.* **2011**, *11* (8), 3370.
(17) Polini, M.; Asgari, R.; Borghi, G.; Barlas, Y.; Pereg-Barnea, T.; MacDonald, A. H. *Phys. Rev. B* **2008**, *77* (8), 081411.
(18) Ju, L.; Geng, B.; Horng, J.; Girit, C.; Martin, M.; Hao, Z.; Bechtel, H. A.; Liang, X.; Zettl, A.; Shen, Y. R.; Wang, F. *Nat. Nanotechnol.* **2011**, *6* (10), 630.
(19) Yan, H.; Li, X.; Chandra, B.; Tulevski, G.; Wu, Y.; Freitag, M.; Zhu, W.; Avouris, P.; Xia, F. *Nat. Nanotechnol.* **2012**, *7* (5), 330.
(20) Yan, H.; Li, Z.; Li, X.; Zhu, W.; Avouris, P.; Xia, F. *Nano Lett.* **2012**, *12* (7), 3766.
(21) Chen, J. N.; Badioli, M.; Alonso-Gonzalez, P.; Thongrattanasiri, S.; Huth, F.; Osmond, J.; Spasenovic, M.; Centeno, A.; Pesquera, A.;

Godignon, P.; Elorza, A. Z.; Camara, N.; de Abajo, F. J. G.; Hillenbrand, R.; Koppens, F. H. L. *Nature* **2012**, *487* (7405), 77.
(22) Fei, Z.; Rodin, A. S.; Andreev, G. O.; Bao, W.; McLeod, A. S.; Wagner, M.; Zhang, L. M.; Zhao, Z.; Thiemens, M.; Dominguez, G.; Fogler, M. M.; Castro Neto, A. H.; Lau, C. N.; Keilmann, F.; Basov, D. N. *Nature* **2012**, *487* (7405), 82.
(23) Fang, Z.; Thongrattanasiri, S.; Schlather, A.; Liu, Z.; Ma, L.; Wang, Y.; Ajayan, P. M.; Nordlander, P.; Halas, N. J.; García de Abajo, F. J. *ACS Nano* **2013**, *7* (3), 2388−2395.
(24) Wendler, L.; Haupt, R. *J. Phys. C: Solid State Phys.* **1986**, *19* (11), 1871.
(25) Arakelian, V. H.; Hovsepian, N. M. *Phys. Status Solidi B* **1991**, *164* (1), 147−155.
(26) Li, X. S.; Cai, W. W.; An, J. H.; Kim, S.; Nah, J.; Yang, D. X.; Piner, R.; Velamakanni, A.; Jung, I.; Tutuc, E.; Banerjee, S. K.; Colombo, L.; Ruoff, R. S. *Science* **2009**, *324* (5932), 1312.
(27) Li, X. S.; Magnuson, C. W.; Venugopal, A.; An, J. H.; Suk, J. W.; Han, B. Y.; Borysiak, M.; Cai, W. W.; Velamakanni, A.; Zhu, Y. W.; Fu, L. F.; Vogel, E. M.; Voelkl, E.; Colombo, L.; Ruoff, R. S. *Nano Lett.* **2010**, *10* (11), 4328.
(28) Novoselov, K. S.; Geim, A. K.; Morozov, S. V.; Jiang, D.; Katsnelson, M. I.; Grigorieva, I. V.; Dubonos, S. V.; Firsov, A. A. *Nature* **2005**, *438* (7065), 197−200.
(29) Christensen, J.; Manjavacas, A.; Thongrattanasiri, S.; Koppens, F. H. L.; García de Abajo, F. J. *ACS Nano* **2011**, *6* (1), 431−440.
(30) Falkovsky, L. A.; Varlamov, A. A. *Eur. Phys. J. B* **2007**, *56* (4), 281−284.
(31) Palik, E. D. *Handbook of Optical Constants of Solids*; Elsevier: New York, 1997.
(32) Fei, Z.; Andreev, G. O.; Bao, W.; Zhang, L. M.; A, S. M.; Wang, C.; Stewart, M. K.; Zhao, Z.; Dominguez, G.; Thiemens, M.; Fogler, M. M.; Tauber, M. J.; Castro-Neto, A. H.; Lau, C. N.; Keilmann, F.; Basov, D. N. *Nano Lett.* **2011**, *11* (11), 4701.
(33) Purcell, E. M. *Phys. Rev.* **1946**, *69* (11−1), 681−681.
(34) Ruppin, R. *Phys. Lett. A* **2002**, *299* (2−3), 309−312.
(35) de Leon, N. P.; Shields, B. J.; Yu, C. L.; Englund, D. E.; Akimov, A. V.; Lukin, M. D.; Park, H. *Phys. Rev. Lett.* **2012**, *108* (22), 226803.
(36) Kuttge, M.; García de Abajo, F. J.; Polman, A. *Nano Lett.* **2009**, *10* (5), 1537−1541.
(37) Yan, H.; Low, T.; Zhu, W.; Wu, Y.; Freitag, M.; Li, X.; Guinea, F.; Avouris, P.; Xia, F. *arXiv:1209-1984v1*.